Tellus (1980), *32*, 124–130

A diagnostic scale-interaction study employing a horizontal filtering technique

By EERO HOLOPAINEN and PERTTI NURMI, *Department of Meteorology, University of Helsinki, Hallituskatu 11-13, 00100 Helsinki 10, Finland*

(Manuscript received June 11, 1979)

ABSTRACT

The present paper is a continuation of the paper by Holopainen and Nurmi (1979), in which an example of a scale-interaction study employing a horizontal filtering technique was reported. Here we apply the same technique to large material (upper wind observations at 300 mb from the British Isles in 1961–65) to investigate some statistical properties of the horizontal "sub-grid" ($L < L_f \sim 400$ km) force $\mathcal{A}^H$. To illustrate the effect qualitatively the technique is also applied to some schematic flow patterns.

The results show that $\mathcal{A}^H$ cannot be parametrized in terms of the smoothed flow with expressions (Fickian scheme, Smagorinsky's (1963) scheme, Leith's (1969) scheme) commonly used in the numerical models for the lateral frictional force.

The mean effect of $\mathcal{A}^H$ on the kinetic energy of the smoothed flow ("lateral dissipation") turns out to be practically zero, whereas all the three parametrization schemes indicate an energy cascade from resolved to unresolved scales. The correlation between the 3464 instantaneous values of observed and parametrized "dissipation" is almost zero.

1. Introduction

In a recent article, the present authors (Holopainen and Nurmi, 1979; hereafter referred to as A) investigated the effects of horizontal unresolved processes in one particular synoptic case. A horizontal filtering technique was used for splitting the observed flow pattern, analyzed with the aid of ordinary upper-air data from the data-rich area of Northern Europe, into a large-scale component and a small-scale component, the dividing wavelength being about 400 km. It was found that in this case the smoothed (large-scale) flow was actually accelerated by the smaller-scale motions, whereas the expressions normally used for parametrization of these processes all gave a decelerating effect.

As a logical continuation of A, we in this paper make use of a large number of atmospheric situations and examine the statistics of the small-scale force and its effect on the kinetic energy of the large-scale flow. As in A we also here compare the small-scale effects obtained from observations with the corresponding quantities obtained by the different parametrization schemes.

In Section 2 we repeat from A the general expression for the horizontal force due to unresolved scales, and also the corresponding formulas from the commonly used parametrization methods. The filter used is described in Section 3. In Section 4 we apply these formulas and the filter to certain simple, schematic flow patterns in order to have some qualitative feeling about the forces under study. The results from the real data analysis are presented in Section 5.

2. General expressions for sub-grid forcing and some parametrization formulae

The balance equation of an arbitrary quantity s can, with pressure as a vertical coordinate, be written in the form (for more detailed discussion, see A):

$$\frac{\partial s}{\partial t} + \nabla \cdot s\mathbf{V} + \frac{\partial}{\partial p} s\omega = S \tag{1}$$

0040-2826/80/020124-07$02.50/0

where S is the intensity of the source of s. For a smoothed (filtered) field $\hat{s}$, (1) can be written as

$$\frac{\partial \hat{s}}{\partial t} + \nabla \cdot \hat{s}\hat{V} + \frac{\partial}{\partial p}\hat{s}\hat{\omega} = \hat{S} + A_s \tag{2}$$

where

$$A_s = A_s^H + A_s^V \tag{3}$$

when

$$A_s^H = -\nabla \cdot (\widehat{sV} - \hat{s}\hat{V}) \tag{4}$$

$$A_s^V = -\frac{\partial}{\partial p}(\widehat{s\omega} - \hat{s}\hat{\omega}) \tag{5}$$

Equation (2) for the smoothed flow is exactly the same as (1) for the unsmoothed flow except that every quantity in (1) is replaced by the corresponding smoothed quantity and a new term A_s appears representing the net effect of unresolved (sub-grid) scales ($L < L_f$) on the resolved scales (L $>$ L_f), the "grid scale" L_f depending upon the filter used (see Section 3).

When the above general expression is applied to the horizontal momentum, we get from (4) for the components of the force due to horizontal sub-grid scale motions the expressions

$$A_{x0}^H = -\frac{\partial}{\partial x}(\widehat{uu} - \hat{u}\hat{u}) - \frac{\partial}{\partial y}[\widehat{uv} - \hat{u}\hat{v}) \tag{6a}$$

$$A_{y0}^H = -\frac{\partial}{\partial x}(\widehat{uv} - \hat{u}\hat{v}) - \frac{\partial}{\partial y}[\widehat{vv} - \hat{v}\hat{v}) \tag{6b}$$

In the following, the right-hand side of (6) is evaluated from observations. Therefore, A_{x0}^H and A_{y0}^H may be referred to as the components of the "observed" horizontal frictional force $\mathcal{A}_0^H = A_{x0}^H \mathbf{i} + A_{y0}^H \mathbf{j}$.

The following three formulations are perhaps the most common among those used in numerical models to represent the force due to the sub-grid scale horizontal processes:

(a) $\mathcal{A}_F^H$: *Fickian formulation*

$$A_{xF}^H = a_F \nabla^2 \hat{u} \tag{7a}$$

$$A_{yF}^H = a_F \nabla^2 \hat{v} \tag{7b}$$

where a_F = constant

(b) $\mathcal{A}_S^H$: *Smagorinsky's (1963) formulation*

$$A_{xS}^H = a_S\left(\frac{\partial}{\partial x}(DD_T) + \frac{\partial}{\partial y}(DD_S)\right) \tag{8a}$$

$$A_{yS}^H = a_S\left(\frac{\partial}{\partial x}(DD_S) - \frac{\partial}{\partial y}(DD_T)\right) \tag{8b}$$

where

$$D_T = \frac{\partial \hat{u}}{\partial x} - \frac{\partial \hat{v}}{\partial y}, \quad D_S = \frac{\partial \hat{v}}{\partial x} + \frac{\partial \hat{u}}{\partial y},$$

$$D = (D_T^2 + D_S^2)^{1/2}$$

and a_S is a constant.

(c) $\mathcal{A}_L^H$: *Leith's (1969) formulation*

$$A_{xL}^H = a_L |\nabla \hat{\zeta}| \nabla^2 \hat{u} \tag{9a}$$

$$A_{yL}^H = a_L |\nabla \hat{\zeta}| \nabla^2 \hat{v} \tag{9b}$$

where

$\hat{\zeta} = \dfrac{\partial \hat{v}}{\partial x} - \dfrac{\partial \hat{u}}{\partial y}$ and a_L is a constant.

If the filtered velocity field is known, the direction of $\mathcal{A}_F^H$, $\mathcal{A}_S^H$ and $\mathcal{A}_L^H$ can be determined without specification of the numerical values a_F, a_S and a_L.

Our purpose with this paper is to discuss, on the basis of real data, the characteristics of the "observed" $\mathcal{A}_0^H$ and its relationship with $\mathcal{A}_F^H$, $\mathcal{A}_S^H$ and $\mathcal{A}_L^H$.

3. The filter

The filter used here is the same as employed in A. Assuming that the original fields are given in a regular two-dimensional grid, our filter is given by the weights:

$$\begin{array}{ccccc} \frac{1}{256} & \frac{4}{256} & \frac{6}{256} & \frac{4}{256} & \frac{1}{256} \\ \frac{4}{256} & \frac{16}{256} & \frac{24}{256} & \frac{16}{256} & \frac{4}{256} \\ \frac{6}{256} & \frac{24}{256} & \frac{36}{256} & \frac{24}{256} & \frac{6}{256} \\ \frac{4}{256} & \frac{16}{256} & \frac{24}{256} & \frac{16}{256} & \frac{4}{256} \\ \frac{1}{256} & \frac{4}{256} & \frac{6}{256} & \frac{4}{256} & \frac{1}{256} \end{array}$$

The extent to which a function of the form $C e^{i(k_x x + k_y y)}$ is affected by the filter (in the case of $\Delta x = \Delta y = 67$ km) is seen in Fig. 1. It is noticed that the filter is essentially quasi-isotropic. The response function is 0.5 at the wavelength of 370 km. We may thus say that the "grid scale" determined by the filter is $L_f \sim 400$ km (this filter "grid scale" should not be mixed with $\Delta x = \Delta y =$ 67 km mentioned above!). In the subsequent analysis, the separation wavelength between resolved (explicit) and unresolved ("sub-grid") scales is

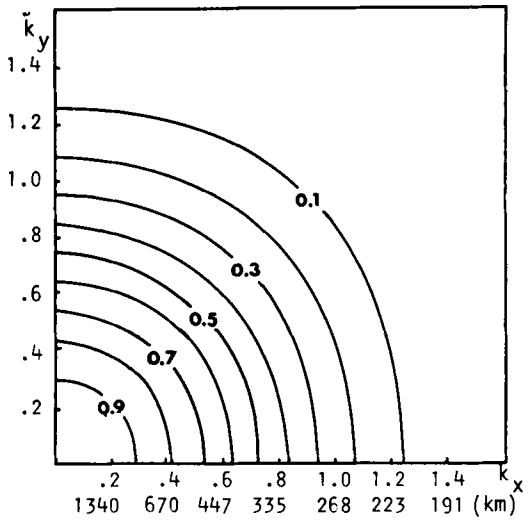

Fig. 1. The wave number response of the filter used.

thus $L_f \sim 400$ km, which roughly corresponds to the resolution, with which the atmospheric large-scale flow can be described from observations over most parts of the globe now and in the future.

4. The force $\mathcal{A}^H$ in some schematic flow patterns

Before studying the horizontal "frictional" force $\mathcal{A}^H$ on the basis of real data, it is illustrative to examine its characteristics in some simple, schematic flow patterns. Fig. 2 shows four hypothetical streamline patterns and the fields of $\mathcal{A}_0^H$ and $\mathcal{A}_F^H$; the fields of $\mathcal{A}_S^H$ and $\mathcal{A}_L^H$ are almost identical to those of $\mathcal{A}_F^H$ and are therefore not shown.

The first flow pattern (case a) describes a strong westerly jet stream with a confluent/diffluent character in the western/eastern part of the area and with a maximum speed of *ca.* 80 m s^{-1}. In this case $\mathcal{A}_0^H$ is determined mainly by the longitudinal "stresses" $\widehat{uu} - \hat{u}\hat{u}$. In the diffluence area the effect of $\mathcal{A}_0^H$ is clearly seen to be acceleration of the smoothed flow (as already demonstrated in the case study reported in A), whereas in the confluence area the situation is quite the opposite. In the diffluence area the "Fickian" force $\mathcal{A}_F^H$ acts in an opposite direction to $\mathcal{A}_0^H$ (as was the case in A), while in the confluence area their effects are quite similar. The situation in the center of the area corresponds to a case of a straight zonal jet. We notice that here $\mathcal{A}_0^H = 0$ while $\mathcal{A}_F^H$ has a definite decelerating effect on the jet.

The second example (case b) in Fig. 2 represents a westerly jet stream with a sharp trough of meridional orientation in the center of the area. The filtering effectively takes away this trough while leaving the flow field elsewhere practically untouched. In the western and eastern parts of the area $\mathcal{A}_0^H$ is, accordingly, practically zero. The main contribution to the relatively large values of $\mathcal{A}_0^H$ ($\approx \mathcal{A}_{0y}^H \hat{j}$) in the center meridian comes from the "stress" $\widehat{vv} - \hat{v}\hat{v}$, which has its maximum at the latitude of the jet core. The field of $\mathcal{A}_F^H$ is again seen to be completely different from that of $\mathcal{A}_0^H$. A small modification of this example is obtained by specifying the zonal wind component as a constant everywhere; in this case we would get zero value for $\mathcal{A}_0^H$, but not for $\mathcal{A}_F^H$, in the whole area.

The next example (case c) represents a broad trough in a flow which has diffluence/confluence features in the western/eastern part of the area. The resulting field of $\mathcal{A}_0^H$ can be qualitatively understood as a combination of the features in cases (a) and (b). The magnitude of $\mathcal{A}_0^H$ is, however, much smaller than in the previous situations. This results from the fact that the total flow is already relatively smooth.

The last schematic flow pattern (case d) in Fig. 2 represents a circular low. The "observed" force $\mathcal{A}_0^H$ is in this case directed outwards from the centre. The physical explanation of this is that the centrifugal force which can be described by the smoothed flow is smaller than the smoothed centrifugal force ($\hat{V}^2/R < \widehat{V^2}/R$, where R = the distance from the center of the low) and, accordingly, the difference has to appear as an outward-directed "sub-grid scale" force in the equations of motion for the smoothed flow. The Fickian force $\mathcal{A}_F^H$ has a decelerating effect on the mean flow and is completely uncorrelated with $\mathcal{A}_0^H$.

In light of the above schematic examples, it can be expected that also in real data study, reported in the next section, correlation between $\mathcal{A}_0^H$ and the different parametrizations $\mathcal{A}_F^H$, $\mathcal{A}_S^H$ and $\mathcal{A}_L^H$ may not be very high.

5. Results obtained using real data

5.1. *Data and the method of analysis*

Calculations of $\mathcal{A}_0^H$ should of course be preferably done from data of high horizontal resolution but we do not have such data at our disposal. However, over the European area with a good network of upper-air stations, the horizontal analyses made

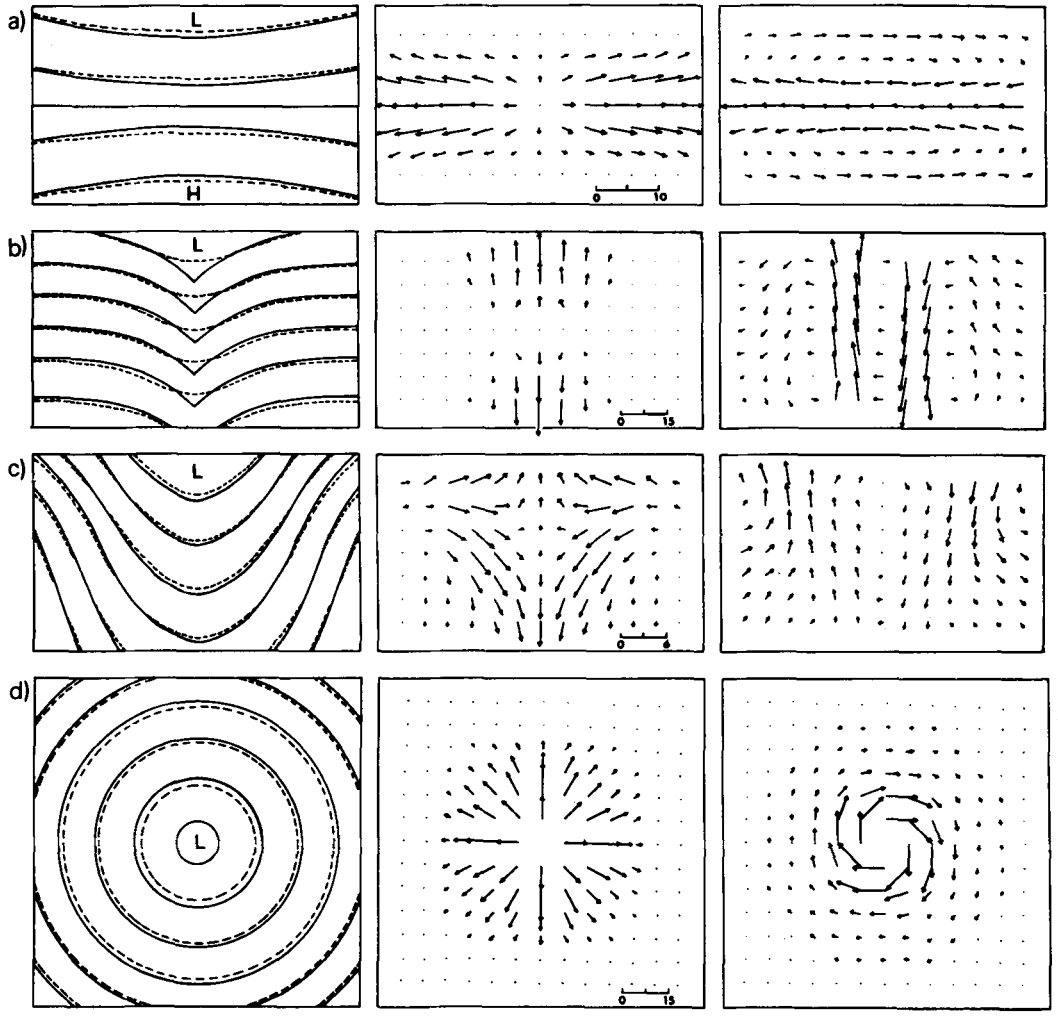

Fig. 2. The sub-grid scale force A_0^H and the Fickian force A_F^H in some schematic flow patterns. In each of the case a–d, the figure to the left shows the stream function for the total flow (continuous line) and for the smoothed flow (dashed line). The figure in the middle shows A_0^H (scale given in 10^{-4} m s^{-2}) and that to the right A_F^H (scale arbitrary). The rectangular area is *ca.* 1000 km × 500 km.

from ordinary upper-wind observations certainly contain (in contrast to areas with a sparse network of stations) a lot of information about the scales smaller than 400 km. It is therefore of interest to see what kind of effect on the smoothed flow is exerted by these features, which admittedly are only a part of the total "sub-grid" scale phenomena in the case of $L_f \sim 400$ km.

The data used here are the twice-daily wind observations at 300 mb for the period 1961–65 from the six upper-wind stations seen in Fig. 3. The number of synoptic cases with complete observations at all six stations during this period was 3464.

The analysis of the horizontal variation of the wind components was done by fitting a second-order polynomial to the observations at the stations. The values of the polynomials, interpreted to represent the total flow, were read off at the points seen in Fig. 3 and smoothed by the filter discussed earlier, whereafter the "stresses" $\widehat{uu} - \hat{u}\hat{u}$, $\widehat{uv} - \hat{u}\hat{v}$, $\widehat{vv} - \hat{v}\hat{v}$, the "observed" force A_0^H and the direction of A_F^H, A_S^H and A_L^H could be determined.

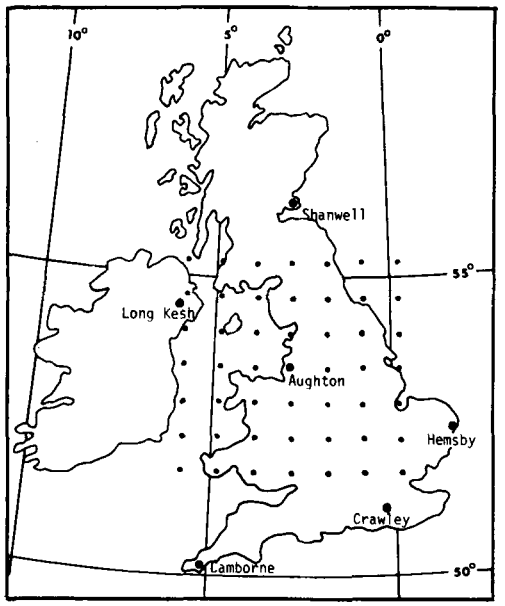

Fig. 3. The network of aerological stations and the grid used in calculations.

5.2. *Stresses* $\widehat{uu} - \hat{u}\hat{u}$, $\widehat{uv} - \hat{u}\hat{v}$, $\widehat{vv} - \hat{v}\hat{v}$

Primary quantities in the calculations of the "observed" force $\mathcal{A}_0^H$ (see Eq. (6)) are the quantities $\widehat{uu} - \hat{u}\hat{u}$, $\widehat{uv} - \hat{u}\hat{v}$ and $\widehat{vv} - \hat{v}\hat{v}$ (which formally correspond to the Reynolds' stresses $\overline{u'^2}$, $\overline{u'v'}$, $\overline{v'^2}$ in the classical discussions of turbulence). The statistics of these "stresses", as calculated from our material, do not vary very much in the area of Fig. 3. Therefore, they are in Table 1 given only for one grid point.

Considering first the mean values we notice a kind of isotropy: those of $\widehat{uu} - \hat{u}\hat{u}$ and $\widehat{vv} - \hat{v}\hat{v}$ are of the same order of magnitude while that of $\widehat{uv} - \hat{u}\hat{v}$ is practically zero. The standard deviations of all three "stresses" are rather similar, which means that in most synoptic situations there is no isotropy present. The large values of the standard deviations further mean that in many cases also $\widehat{uu} - \hat{u}\hat{u}$ and $\widehat{vv} - \hat{v}\hat{v}$ are negative, which of course is never the case with the corresponding classical Reynolds' stresses.

A point of some interest in Table 1 is that both the mean value and standard deviation of $\widehat{vv} - \hat{v}\hat{v}$ are slightly larger than those of $\widehat{uu} - \hat{u}\hat{u}$. This means that the smoothing has a larger effect on the meridional than on the zonal wind component. In other words there is more energy in the meridional than in the zonal component in the unfiltered fields at high wave numbers.

Table 1. *Mean values and standard deviations (SD) of the horizontal "stresses" during 1961–65 for the central grid point in Fig. 3. Units:* $m^2\ s^{-2}$

	$\widehat{uu} - \hat{u}\hat{u}$	$\widehat{uv} - \hat{u}\hat{v}$	$\widehat{vv} - \hat{v}\hat{v}$
Mean	7.0	−0.2	9.0
SD	8.4	7.2	11.6

5.3. *Observed and simulated forces and their correlations*

In this section we will consider, componentwise, the time-mean values, standard deviations and mutual correlations of the forces $\mathcal{A}_0^H$, $\mathcal{A}_F^H$, $\mathcal{A}_S^H$ and $\mathcal{A}_L^H$. In order to be able to compare $\mathcal{A}_0^H$ with $\mathcal{A}_F^H$, $\mathcal{A}_S^H$ and $\mathcal{A}_L^H$ (without entering the discussion of the coefficients a_F, a_S and a_L in eqs. (7)–(9)) we have scaled the latter quantities in such a way that their RMS (root mean square) values, when combining both components, is the same as that of $\mathcal{A}_0^H$. This scaling affects the mean values and SD values but not the correlation coefficients.

In order to see better the effect of calculated forces we consider them in a "natural" coordinate system, in which any vector is split into components parallel and normal to $\hat{V}$.

Considering first the characteristics of $\mathcal{A}_0^H$ we notice from Table 2 that its time-mean value is practically zero. Its typical magnitude in instantaneous cases, judged from the SD values, corresponds to a force caused, through the coriolis effect, by a velocity of about 0.5 ms^{-1}, and is thus rather small. It is probably an underestimate of the magnitude of the true force $\mathcal{A}_o^H$ because our data contain only a part of the features at scales smaller than L_f.

Considering now $\mathcal{A}_F^H$, $\mathcal{A}_S^H$ and $\mathcal{A}_L^H$ we observe from Table 2 that all of them have a large negative mean parallel component (which means a decelerating effect on the smoothed flow), whereas the mean normal component is close to zero.

The most interesting question concerning $\mathcal{A}_F^H$, $\mathcal{A}_S^H$ and $\mathcal{A}_L^H$ is, of course, how well they simulate the day-to-day variation of $\mathcal{A}_0^H$. This can be partially answered with the aid of the correlation matrix seen in Table 3. It is apparent that these three expressions correlate relatively well with each other but have practically nothing to do (correlation coefficients ~0.1) with the corresponding components

Table 2. *Mean values and standard deviations (SD) of the "observed" force $\mathcal{A}_0^H$ (in 10^{-5} m s^{-2}) and the corresponding values obtained by the three parametrization schemes. The latter values are scaled so as to give the same RMS value as $\mathcal{A}_0^H$. N = 3464*

		$\mathcal{A}_0^H$	$\mathcal{A}_F^H$	$\mathcal{A}_S^H$	$\mathcal{A}_L^H$
Mean,	parallel	0.11	−2.52	−1.82	−2.25
	normal	−0.14	0.12	0.10	0.07
SD,	parallel	5.29	5.22	5.47	5.71
	normal	4.39	3.67	3.73	3.08

Table 3. *Correlation coefficients between the "observed" force $\mathcal{A}_0^H$ and the corresponding values obtained by the three parametrization schemes. N = 3464*

		$\mathcal{A}_F^H$	$\mathcal{A}_S^H$	$\mathcal{A}_L^H$
$\mathcal{A}_0^H$	parallel	0.07	0.08	0.10
	normal	0.11	0.06	0.17
$\mathcal{A}_F^H$	parallel		0.82	0.88
	normal		0.77	0.87
$\mathcal{A}_S^H$	parallel			0.80
	normal			0.74

of $\mathcal{A}_0^H$; this is true for both components of the force.

5.4. *The effect of $\mathcal{A}^H$ on the kinetic energy of the smoothed flow*

Table 4 shows the mean values and standard deviations of $\hat{V}\cdot\mathcal{A}^H$, the work done ("lateral dissipation") by the forces $\mathcal{A}_0^H$, $\mathcal{A}_F^H$, $\mathcal{A}_S^H$ and $\mathcal{A}_L^H$ on the smoothed flow. Positive (negative) mean values indicate a mean increase (decrease) of the kinetic energy of $\hat{V}$. The correlation matrix (corresponding to that in Table 3) is given in Table 5.

According to Table 4 the "observed" force $\mathcal{A}_0^H$ gives, on average, a small increase of kinetic energy of the smoothed flow. The large value of the standard deviation shows that in individual synoptic situations $\hat{V}\cdot\mathcal{A}_0^H$ is practically as often negative as it is positive and that, statistically, the mean value is not significantly different from zero. All three parametrizations of $\mathcal{A}^H$ give, in the mean, a loss of the kinetic energy of the smoothed flow. The large standard deviations indicate, however, that their effect varies from case to case even by sign. The correlation matrix in Table 5 shows, in conformity with the results presented in Section 5.3,

Table 4. *Mean values and standard deviations (SD) of the work done by the "observed" force $\mathcal{A}_0^H$, and by the forces determined from the three parametrization schemes. The latter values are scaled so as to give the same RMS value as $\hat{V}\cdot\mathcal{A}_0^H$. Unit for $\hat{V}\cdot\mathcal{A}_0^H$: 10^{-4} m^2 s^{-2}*

	$\hat{V}\cdot\mathcal{A}_0^H$	$\hat{V}\cdot\mathcal{A}_F^H$	$\hat{V}\cdot\mathcal{A}_S^H$	$\hat{V}\cdot\mathcal{A}_L^H$
Mean	0.45	−7.84	−5.84	−6.12
SD	18.74	17.03	17.82	17.73

Table 5. *Correlation coefficients between the work done by the force $\mathcal{A}^H$ as "observed" and as determined from the three parametrization schemes*

	$\hat{V}\cdot\mathcal{A}_F^H$	$\hat{V}\cdot\mathcal{A}_S^H$	$\hat{V}\cdot\mathcal{A}_L^H$
$\hat{V}\cdot\mathcal{A}_0^H$	0.03	0.03	0.07
$\hat{V}\cdot\mathcal{A}_F^H$		0.85	0.92
$\hat{V}\cdot\mathcal{A}_S^H$			0.85

that the effects of the three parametrization schemes (particularly those of the Fickian and Leith's scheme) are very similar to each other. On the other hand, they have very little to do with the effect of the "observed" force: the best correlation, 0.07, is given by Leith's scheme, which means explanation of only 0.5 % of the variance of $\hat{V}\cdot\mathcal{A}_0^H$!

If we assume that the calculated time-mean value of $\hat{V}\cdot\mathcal{A}_0^H$ for the British Isles is representative for other regions, too, we conclude that the mean energy cascade due to horizontal "stresses", from scales smaller than L_f (~400 km) to larger scales is practically zero. Assuming that this value of L_f falls into the enstrophy cascade subrange, this result is in accordance with the theories of two-dimensional turbulence. The three parametrization schemes, on the other hand, all give on average a definite energy cascade from resolved to unresolved scales.

6. Discussion

The main result of the present analysis is that the parametrization formulae commonly used in the numerical models of the atmospheric large-scale flow for the representation of friction due to unresolved horizontal eddies, seem to have nothing to do with the corresponding observed force. This result is at first sight amazing. It is, however, in

accordance with the theoretical analysis by Kraichnan (1976) who concluded that "... the theoretical basis for the use of simple eddy viscosities to represent sub-grid scales is substantially insecure".

A question naturally arises whether there is some other simple parametrization of $\mathcal{A}^H$, which could explain the variation of $\mathcal{A}_0^H$ better than $\mathcal{A}_F^H$, $\mathcal{A}_S^H$ and $\mathcal{A}_L^H$. We have made experiments with three additional expressions, one proportional to $-\hat{V}$ (Rayleigh friction), the second proportional to $-|\hat{V}|\hat{V}$ and the third proportional to $(\hat{V}\cdot\nabla)\hat{V}$. The result was that none of these schemes (which in our case do not have any physical justification) gave significantly better correlations with $\mathcal{A}_0^H$ than those seen in Table 5.

A point to be emphasized is that we have here considered the effect of sub-grid scales only somewhat smaller than 400 km. It may be that the forcing effect of scales significantly smaller than 400 km can be parametrized in terms of simple eddy viscosities. On the other hand, our approach is at least partially motivated by the theoretical finding (Kraichnan, 1976) that the main effect of scale interaction on the resolved scales comes from the wavelengths close to L_f. In any case, to study this question in more detail, the horizontal resolution of the data has to be higher than in our sample. For this reason, no detailed statistical analysis (e.g. structural properties in space and time) of the sub-grid scale features has been done here. Only a few general comments will be made in this respect.

The space scale of sub-grid flow pattern $V - \hat{V}$, obtained by the filtering approach used here, is by definition small (<400 km). In the case of jet streams $V - \hat{V}$ typically has a banded structure (as in the example reported in A). The forcing effect V_0^H is typically concentrated in relatively small areas, whereas a major part of the flow is relatively "frictionless". In the Eulerian sense, the dominant scale of time variation of $\mathcal{A}_0^H$ is also likely to be small. In the Lagrangian sense (i.e. following the smoothed flow trajectories) the time scale of its variation is, however, probably close to that of the synoptic disturbances. For this reason this forcing, which depends in a complicated way upon the properties of the flow at resolved scales, cannot be considered a random process.

Since a long series of data with high spatial resolution are almost impossible to obtain, probably the best bases for scale interaction studies employing horizontal filtering techniques are the "data" from high resolution numerical models.

REFERENCES

Holopainen, E. O. and Nurmi, P. 1979. Acceleration of a diffluent jet stream by horizontal sub-grid scale processes—an example of a scale interaction study employing a horizontal filtering technique. *Tellus 31*, 246–253.

Kraichnan, R. H. 1976. Eddy viscosity in two and three dimensions. *J. Atm. Sci. 33*, 1521–1553.

Leith, C. E. 1969. Two dimensional eddy viscosity coefficients. Proc. of the WMO/IUGG symposium on numerical weather prediction in Tokyo Nov. 26–Dec. 4, 1968. Japan Met. Agency, Tokyo.

Smagorinsky, J. 1963. General circulation experiments with the primitive equations. I. The basic experiment. *Mon. Wea. Rev. 91*, 99–164.

ДИАГНОСТИЧЕСКОЕ ИССЛЕДОВАНИЕ ВЗАИМОДЕЙСТВИЙ МЕЖДУ РАЗЛИЧНЫМИ МАСШТАБАМИ С ИСПОЛЬЗОВАНИЕМ МЕТОДИКИ ГОРИЗОНТАЛЬНОЙ ФИЛЬТРАЦИИ

Настоящая статья является продолжением работы Холопайнена и Нурми (1979), в которой был описан пример исследования взаимодействий между различными маштабами, исолрзуюший методику горизонтальной фильтрации. Здесь мы применяем ту же методику к болъшому материалу (наблюдения за ветром на поверхности 300 мб над Британскими островами за 1961–65 гг.) для изучения некоторых статистических свойств горизонтальной "подсеточной" ($L<L_f\sim 400$ км) силы $\mathcal{A}^H$ Для качественной иллюстрации эффекта методика применяется также к некоторым схематическим типам течений.

Результаты показывают, что величина $\mathcal{A}^H$ не может быть параметризована в терминах сглаженного потока с помощью выражений, обычно используемых в численных моделях для горизонтальной силы трения (схема фика, схема Смагоринского (1963), схема Лейса (1969).

Среднее влияние $\mathcal{A}^H$ на кинетическую энергию сглаженного течения ("горизонтальная диссипация") оказывается практически нулевым, в то время как все три схемы параметризации дают каскад энергии от разрешаемых к подсеточным масштабам. Корреляция между 3464 мгновенными величинами наблюдаемой и "параметризованной" диссипации почти нуль.